CORRECTED 17 JULY 2015; SEE LAST PAGE

Reaction of O_2 with Subsurface Oxygen Vacancies on TiO_2 Anatase (101)

Martin Setvín,[1] Ulrich Aschauer,[2]* Philipp Scheiber,[1] Ye-Fei Li,[2] Weiyi Hou,[2] Michael Schmid,[1] Annabella Selloni,[2] Ulrike Diebold[1]†

Oxygen (O_2) adsorbed on metal oxides is important in catalytic oxidation reactions, chemical sensing, and photocatalysis. Strong adsorption requires transfer of negative charge from oxygen vacancies (V_Os) or dopants, for example. With scanning tunneling microscopy, we observed, transformed, and, in conjunction with theory, identified the nature of O_2 molecules on the (101) surface of anatase (titanium oxide, TiO_2) doped with niobium. V_Os reside exclusively in the bulk, but we pull them to the surface with a strongly negatively charged scanning tunneling microscope tip. O_2 adsorbed as superoxo (O_2^-) at fivefold-coordinated Ti sites was transformed to peroxo (O_2^{2-}) and, via reaction with a V_O, placed into an anion surface lattice site as an $(O_2)_O$ species. This so-called bridging dimer also formed when O_2 directly reacted with V_Os at or below the surface.

Molecular O_2 interacts weakly with fully oxidized metal oxides. When excess electrons are present, it adsorbs as an anion in either superoxo (O_2^-), peroxo (O_2^{2-}), or dissociated ($2 \times O^{2-}$) form. The negative charge can be provided by intrinsic defects [e.g., oxygen vacancies (V_Os) or cation interstitials] in a reduced oxide, by doping, or through photoexcitation. Such adsorbed oxygen plays a key role in several technological processes; for example, in oxidation reactions promoted by heterogeneous catalysts, in gas sensors, or in photocatalysis (*1*, *2*). Because of the complexity of technical materials, multiple oxidation states, and the background of lattice oxygen, a molecular-level understanding of O_2 adsorption is just emerging (*3*, *4*). Scanning tunneling microscopy (STM) studies on macroscopic, single-crystalline samples with flat surfaces and controlled defects allow a direct view of adsorbed species. In conjunction with density functional theory (DFT) calculations, these studies provide fundamental insights into a rich surface chemistry (*3*–*9*). However, experimental studies have not focused on anatase that makes up nanophase titania, nor have they addressed the role of subsurface V_Os that are prevalent in this material (*10*, *11*). Here, we show that manipulations with the scanning tunneling microscope tip can be used to (i) locally create surface V_Os, (ii) alter the charge state of adsorbed O_2, and (iii) react adsorbed O_2 with subsurface V_Os to produce an interstitial $(O_2)_O$ species (or bridging O_2 dimer) that has been predicted theoretically.

Our sample was an anatase mineral single crystal, naturally doped with 1.1 atomic % niobium [see the supplementary materials (*12*)], an efficient electron donor. Although the thermodynamically stable rutile phase [especially the (110) surface of single crystals] has been extensively used as a model surface (*3*, *4*, *13*), nanophase TiO_2, which is often used in applications, usually consists of anatase (*14*). Anatase is also frequently referred to as photocatalytically more active, and several studies (*15*–*17*) have shown that substantial amounts of O_2 are present on the surface of photoirradiated anatase, but not on rutile. This could be caused by the different response to

[1]Institute of Applied Physics, Vienna University of Technology, Wiedner Hauptstrasse 8-10/134, 1040 Vienna, Austria. [2]Department of Chemistry, Princeton University, Frick Laboratory, Princeton, NJ 08544, USA.

*Present address: ETH Zurich, Materials Theory, Wolfgang-Pauli-Strasse 27, 8093 Zürich, Switzerland.
†Corresponding author. E-mail: diebold@iap.tuwien.ac.at

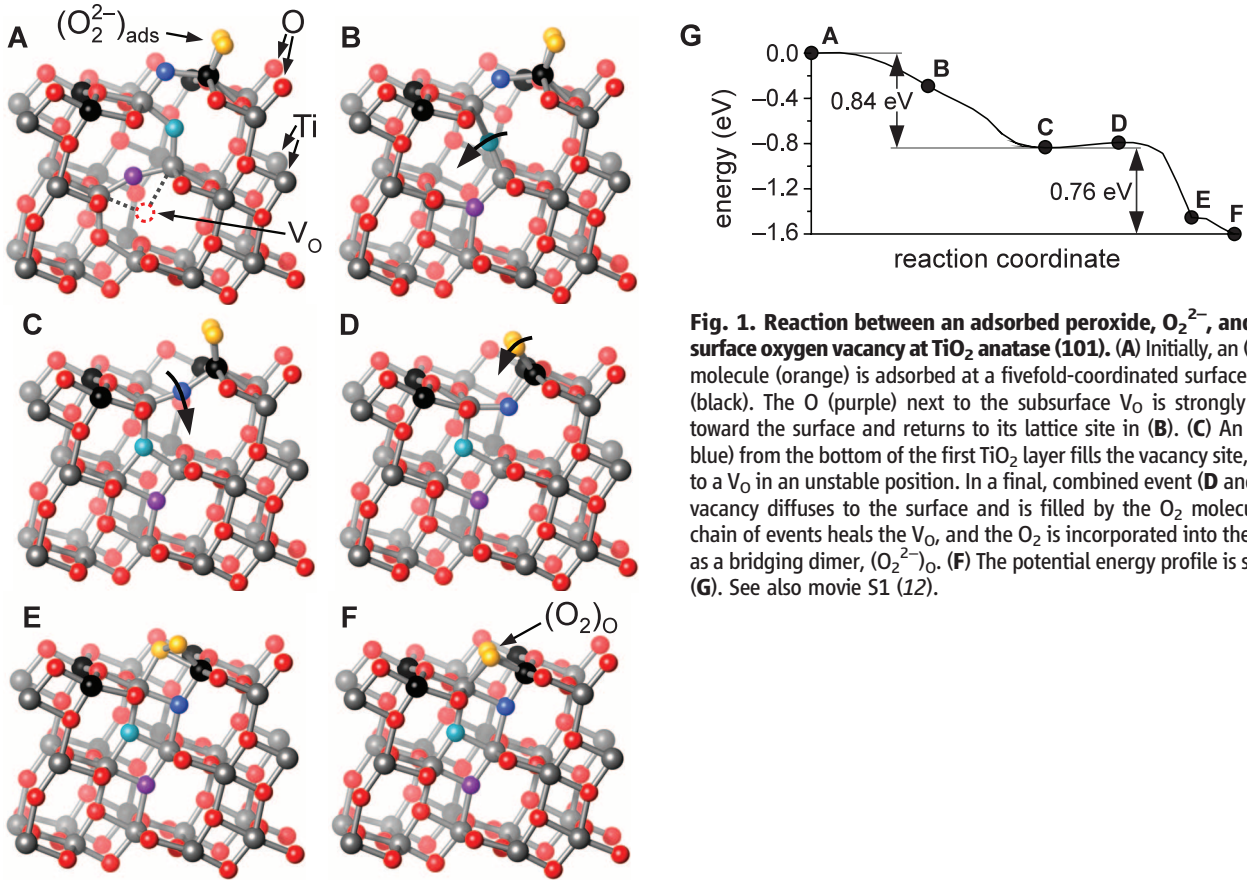

Fig. 1. Reaction between an adsorbed peroxide, O_2^{2-}, and a subsurface oxygen vacancy at TiO_2 anatase (101). (**A**) Initially, an $(O_2^{2-})_{ads}$ molecule (orange) is adsorbed at a fivefold-coordinated surface Ti atom (black). The O (purple) next to the subsurface V_O is strongly relaxed toward the surface and returns to its lattice site in (**B**). (**C**) An O (light blue) from the bottom of the first TiO_2 layer fills the vacancy site, leading to a V_O in an unstable position. In a final, combined event (**D** and **E**), the vacancy diffuses to the surface and is filled by the O_2 molecule. This chain of events heals the V_O, and the O_2 is incorporated into the surface as a bridging dimer, $(O_2^{2-})_O$. (**F**) The potential energy profile is shown in (**G**). See also movie S1 (*12*).

photoexcitation, notably by long-lived photoexcited electrons present in anatase but not in rutile (*18*), which provide the charge for oxygen adsorption, or by the specific surface properties of anatase (*2*, *19*).

In contrast to TiO_2 rutile (110), V_Os are not stable at the surface of anatase (*10*, *11*). When surface V_Os are created by electron bombardment, they move into the bulk at temperatures as low as 200 K (*11*). In DFT calculations for an anatase slab with a subsurface V_O (which provides negative charge), O_2 adsorbs molecularly at fivefold-coordinated surface (Ti_{5c}) atoms (Fig. 1A) as a peroxo (O_2^{2-}) and a superoxo (O_2^-) species at low and high coverages (*20*), respectively. Ti interstitials, which lead to dissociation of O_2 at rutile (110) (*5*), have the same effect on anatase (101) (*21*).

A peroxide $(O_2^{2-})_{ads}$ adsorbed in the vicinity of a subsurface V_O (Fig. 1A) induces substantial structural relaxation, suggesting the existence of an energetically more favorable configuration. In first-principles molecular dynamics (FPMD) simulations (at 220 K), we observed the cascade of events shown in Fig. 1, B to E. In the resulting structure, the O_2 takes the position of a twofold-coordinated O (O_{2c}) atom in a bridging, side-on η^2 configuration; in Kröger-Vink notation, we refer to this species as an $(O_2)_O$. The $(O_2)_O$ retains a bond length of 1.46 Å, characteristic of O_2^{2-} (*20*). This species (often referred to as interstitial or bridging O_2) has been predicted consistently in theoretical calculations of oxygen in or on anatase (*22*, *23*) and has been proposed to be an important intermediate in the photocatalytic splitting of H_2O.

If such an $(O_2)_O$ species exists, it should also form when an O_2 directly reacts with a surface V_O. To test this hypothesis, we prepared surface V_Os on anatase (101) (Fig. 2). In previous work, we created such V_Os by bombarding TiO_2 with electrons (*11*, *24*). Here, we find that identical defects can be generated by the scanning tunneling microscope tip. Figure 2 shows STM images after scanning with high bias voltage and tunneling current. The bright spots within a well-defined area (Fig. 2A) are the same V_Os as

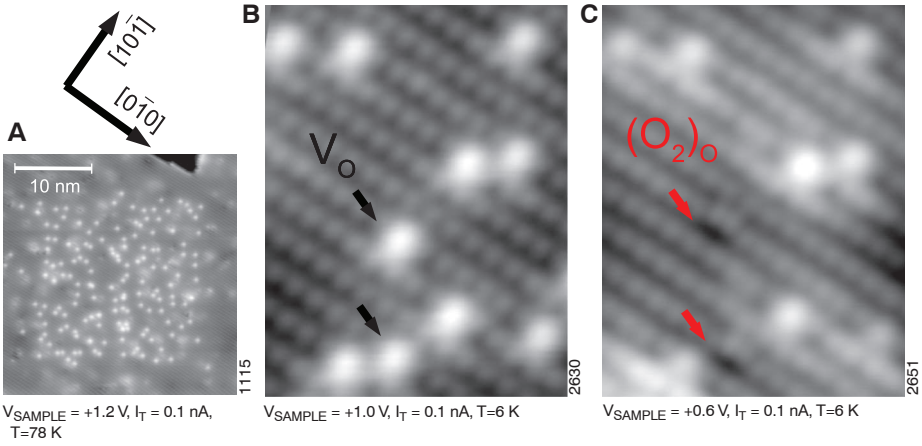

Fig. 2. Interaction of O_2 with surface oxygen vacancies (V_O) on TiO_2 anatase (101). In reduced anatase, V_Os are normally present within the bulk. In (**A**), these were pulled to the surface locally by scanning the center with a high sample bias of +5.2 V. In the high-resolution images of the same area before (**B**) and after (**C**) dosing 0.15 Langmuir (L) O_2 at 45 K, the arrows point out V_Os that reacted with O_2, forming the $(O_2)_O$ configuration shown in Fig. 1F. I_T, tunneling current; T, temperature.

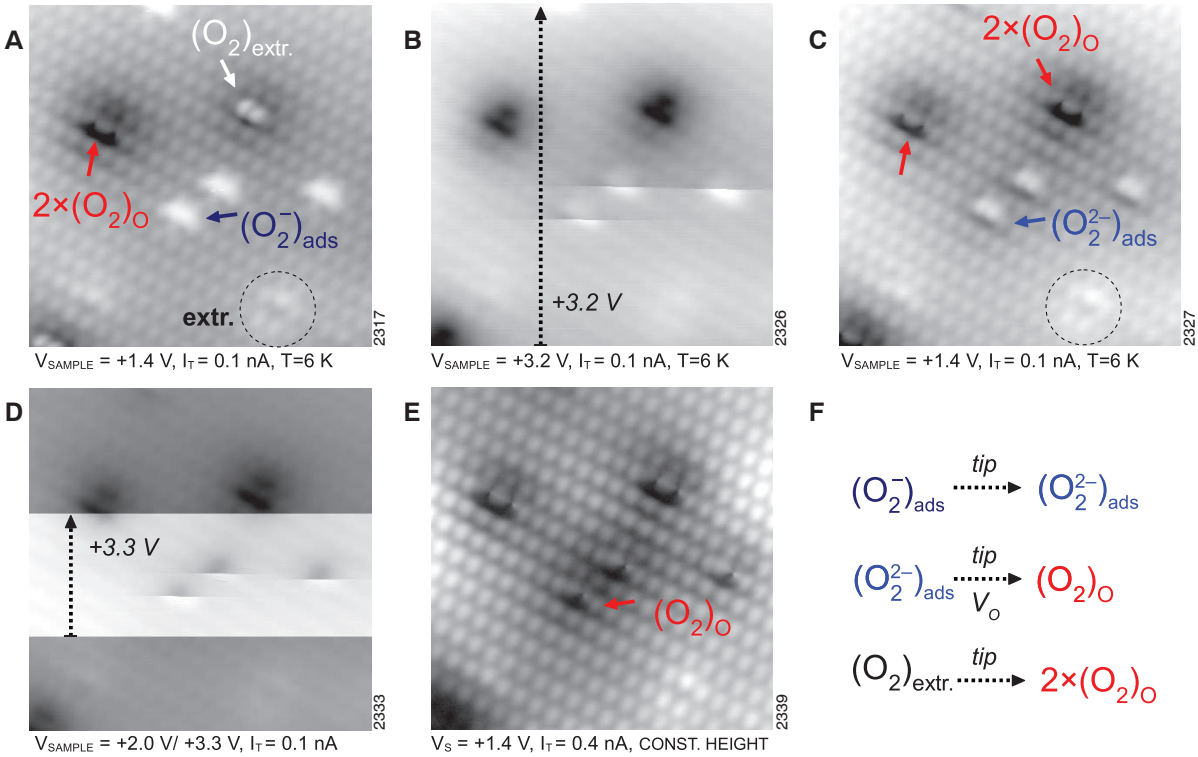

Fig. 3. Scanning tunneling microscope tip–induced conversion of adsorbed O_2. Sequence of STM images of the same area of an anatase (101) surface after exposure to 20 L O_2 at 105 K. (**A**) Various configurations of O_2: at regular sites, $(O_2^-)_{ads}$; at the position of lattice oxygen, $(O_2)_O$; and at the dopants, $(O_2)_{extr}$. The dopants are likely Nb; one of them is marked with a dashed circle. After increasing the sample bias voltage to +3.2 V (**B**), the $(O_2)_{extr}$ is converted to two $(O_2)_O$ species and the $(O_2^-)_{ads}$ to an intermediate species, likely a peroxo ion, $(O_2^{2-})_{ads}$ (**C**). An additional scan with V_{sample} = +3.3 V (**D**), converts each $(O_2^{2-})_{ads}$ into one $(O_2)_O$ species (**E**). (**F**) Overview of the tip-induced processes.

the ones generated by electron irradiation (*11*). After dosing with O_2 (Fig. 2), some of the V_Os were replaced by double spots located at O_{2c} sites. Their appearance agrees well with calculated STM images of the $(O_2)_O$ configuration (fig. S4). The $(O_2)_O$ species did not form at temperatures below 20 K, but it readily appeared when O_2 was dosed above 40 K, with a sticking coefficient S near unity. This result roughly fits the DFT-derived activation energy of 47 meV (see Fig. 1G).

When we dosed a surface without such artificially created surface V_Os, we also see the same $(O_2)_O$ configuration, albeit quite rarely (see supplementary materials). Most often, we observed two different O_2 species (Fig. 3). One of them, denoted $(O_2)_{extr}$, is related to the Nb dopant that preferably replaces a surface Ti_{6c} atom (fig. S2 and table S2). These dopants are distributed unevenly at the surface, with an average concentration of 0.5% of a monolayer [(ML), defined as the density of surface Ti_{5c} atoms] and a local variation between 0.1 and 1% ML. In STM, these impurities exhibit a typical triangular shape (Fig. 3A and fig. S1). Upon O_2 exposure at 105 K, bright dimers were found at the position of these extrinsic dopants; they adsorbed with $S \approx 0.1$. In DFT calculations (fig. S3), the adsorption of an O_2 molecule at a Ti_{5c} atom is preferred by 0.12 to 0.15 eV when next to a Nb_{6c} atom.

In addition to $(O_2)_{extr}$, a bright species, labeled $(O_2)_{ads}$, formed with with $S \approx 10^{-4}$ to 10^{-2} when anatase (101) was exposed to O_2 at 100 K. (The higher values were observed on a more reduced crystal.) The $(O_2)_{ads}$ is located at regular Ti_{5c} surface atoms. Its concentration increases linearly with O_2 exposure (fig. S5). The highest coverage observed was 5% ML. For higher exposures, STM imaging becomes difficult; the saturation coverage could be considerably higher.

The $(O_2)_{ads}$ can be converted into other species with the scanning tunneling microscope tip. Figure 3A shows several $(O_2)_{ads}$ and $(O_2)_{extr}$. During scanning at $V_{sample} = +3.2$ V (Fig. 3B), horizontal streaks indicate that the adsorbates were modified by the presence of the tip. (The slow scan direction was from bottom to top.) The $(O_2)_{ads}$ became more dimerlike (Fig. 3C), and the dark contours indicate that this new species carried a more negative charge. When subjecting these intermediate species to a slightly higher voltage (Fig. 3D), a second conversion took place; see Fig. 3E. The resulting species is the $(O_2)_O$ that also formed when an O_2 molecule directly reacted with a surface V_O. (See supplementary materials for more experimental evidence.) Also note that the $(O_2)_{extr}$ was already converted into two $(O_2)_O$ species during the first high-voltage scan (Fig. 3, B and C) and that two $(O_2)_O$ were always produced per one $(O_2)_{extr}$, whereas only one $(O_2)_O$ species resulted from each $(O_2)_{ads}$ (Fig. 3F). For example, the two neighboring $(O_2)_O$ configurations indicated in the initial image (Fig. 3A) resulted from previously scanning an $(O_2)_{extr}$ at high bias. The tip-induced conversion was reproducible on different samples and with different tips at a minimum V_{sample} of +3.3 ± 0.1 V.

From these results, we derive a complete picture of the reaction of O_2 with a reduced TiO_2 anatase (101) surface. When O_2 impinges on the cold (~100 K) sample, it is weakly adsorbed. Stronger adsorption occurs when electrons are transferred from the surface to the molecule. The Nb^{5+} dopants with nearby electrons are populated first, resulting in $(O_2)_{extr}$ species. A molecule can also extract an electron from TiO_2 at a terrace site to form an $(O_2^-)_{ads}$. Adsorbed O_2 species have a high binding energy (*20*) and are immobile in STM.

Although $(O_2)_O$ species form on as-dosed surfaces with subsurface V_Os, their concentration is low. The spontaneous healing process depicted in Fig. 1 happens rarely. V_Os are more stable in the subsurface region than on the surface by ~0.4 eV (*10*). The activation energy for a V_O to hop from the surface to the first subsurface layer ranges from 0.6 to 1.2 eV, and the barrier for the reverse process is higher by ~0.4 eV (*11*). In the bulk, V_Os diffuse with a much lower barrier of ~0.2 eV; thus, they tend to avoid the surface. Although an adsorbed, negatively charged O_2 reverses the energy balance (Fig. 1), the bulk V_Os seldom come close enough to the selvedge for the healing process to take place.

We pulled V_Os to the adsorbate-free surface with a sufficiently negative scanning tunneling microscope tip. Figure S10 shows that this process is clearly field-induced. The field likely reaches into the semiconductor (tip-induced band-bending) and pushes away electrons that are more or less localized around the V_O. This ionizes and destabilizes the vacancy, similar to the effect triggered by draining of electrons via localization at the O_2^{2-} in the FPMD simulations. The threshold bias voltage for this process is 4.5 eV; the process becomes efficient at 5.2 V. The field-induced migration of intrinsic defects within TiO_2 is already used in novel memory devices, but the nature of the mobile species is controversial (*25*). Our results show that V_Os in TiO_2 can be manipulated by high electric fields.

The tip-induced transformations of the adsorbed O_2 species are summarized in Fig. 3F. We propose that, initially, superoxide $(O_2^-)_{ads}$ forms at regular Ti_{5c} sites. These are transformed into peroxide ions; the increase in band-bending observed after the first tip-induced conversion step suggests that the O_2 becomes more negatively charged. A similar, thermally activated transformation occurs if the sample is heated to temperatures between 200 and 300 K (fig. S11). DFT predicts similar adsorption configurations for $(O_2^-)_{ads}$ and $(O_2^{2-})_{ads}$, except for a slightly longer bond length in the peroxide ion (1.33 versus 1.48 Å) (*20*). By hybrid functional calculations (*26*), we found a barrier of ~0.3 eV to transform $(O_2^-)_{ads}$ into the more stable $(O_2^{2-})_{ads}$ species. Once the $(O_2^{2-})_{ads}$ is formed, somewhat higher bias voltages (and/or prolonged exposure to the field) help the adsorbed molecule to merge with a subsurface V_O, resulting in the bridging dimer at a lattice site, $(O_2)_O$. For $(O_2)_{extr}$ near the Nb impurity, the situation is different. $(O_2)_{extr}$ is dissociated by the tip with a threshold voltage of 1.6 to 2.5 V, smaller than the 3.3 ± 0.1 V needed for the $(O_2)_{ads} \rightarrow (O_2)_O$ conversion. Each of the resulting adatoms merges with an O_{2c} atom to form an $(O_2)_O$ species, consistent with the DFT predictions (*23*).

Our results clearly show the importance of subsurface O vacancies in TiO_2 anatase. They also exemplify how the electric field—for example, from a scanning tunneling microscope tip—can be used as an effective tool to control the charge state of photocatalytically active species. The field can induce transformations of adsorbed O_2 that, by merging with a subsurface V_O, ultimately lead to the formation of the $(O_2)_O$ interstitial. This is by far the most stable O_2 species on the anatase surface. $(O_2)_O$ is also an important intermediate in the photooxidation of water (*23*), which suggests that it could contribute to the higher photocatalytic activity of anatase relative to rutile. Thus, manipulating and controlling the $(O_2)_O$ interstitial might be a key to furthering the development of more active O-rich TiO_2 photocatalysts for water oxidation (*27*).

References and Notes

1. A. L. Linsebigler, G. Lu, J. T. Yates, *Chem. Rev.* **95**, 735–758 (1995).
2. M. A. Henderson, *Surf. Sci. Rep.* **66**, 185–297 (2011).
3. Z. Dohnálek, I. Lyubinetsky, R. Rousseau, *Prog. Surf. Sci.* **85**, 161–205 (2010).
4. U. Diebold, *Surf. Sci. Rep.* **48**, 53–229 (2003).
5. S. Wendt *et al.*, *Science* **320**, 1755–1759 (2008).
6. G. A. Kimmel, N. G. Petrik, *Phys. Rev. Lett.* **100**, 196102 (2008).
7. P. Scheiber, A. Riss, M. Schmid, P. Varga, U. Diebold, *Phys. Rev. Lett.* **105**, 216101 (2010).
8. H. Onishi, Y. Iwasawa, *Phys. Rev. Lett.* **76**, 791–794 (1996).
9. N. G. Petrik, G. A. Kimmel, *J. Phys. Chem. C* **115**, 152–164 (2011).
10. Y. He, O. Dulub, H. Cheng, A. Selloni, U. Diebold, *Phys. Rev. Lett.* **102**, 106105 (2009).
11. P. Scheiber *et al.*, *Phys. Rev. Lett.* **109**, 136103 (2012).
12. See supplementary materials on *Science* Online.
13. C. Pang, R. Lindsay, G. Thornton, *Chem. Soc. Rev.* **37**, 2328–2353 (2008).
14. X. Chen, S. S. Mao, *Chem. Rev.* **107**, 2891–2959 (2007).
15. J. Augustynski, *Electrochim. Acta* **38**, 43–46 (1993).
16. A. Sclafani, J. M. Herrmann, *J. Phys. Chem. C* **100**, 13655–13661 (1996).
17. Y. Nakaoka, Y. Nosaka, *J. Photochem. Photobiol. A* **110**, 299–305 (1997).
18. Y. Yamada, Y. Kanemitsu, *Appl. Phys. Lett.* **101**, 133907 (2012).
19. M. Xu *et al.*, *Phys. Rev. Lett.* **106**, 138302 (2011).
20. U. Aschauer, J. Chen, A. Selloni, *Phys. Chem. Chem. Phys.* **12**, 12956–12960 (2010).
21. U. Aschauer, A. Selloni, *Proc. SPIE* **7758**, 77580B (2010).
22. S. Na-Phattalung *et al.*, *Phys. Rev. B* **73**, 125205 (2006).
23. Y.-F. Li, Z. P. Liu, L. Liu, W. Gao, *J. Am. Chem. Soc.* **132**, 13008–13015 (2010).
24. O. Dulub *et al.*, *Science* **317**, 1052–1056 (2007).
25. K. Szot *et al.*, *Nanotechnology* **22**, 254001 (2011).
26. Y.-F. Li, A. Selloni, *J. Am. Chem. Soc.* **135**, 9195–9199 (2013).
27. V. Etacheri, M. K. Seery, S. J. Hinder, S. C. Pillai, *Adv. Funct. Mater.* **21**, 3744–3752 (2011).

Acknowledgments: The experimental work was supported by the Austrian Science Fund (FWF; project F45) and the European Research Council Advanced Grant "OxideSurfaces." The theoretical work was supported by the U.S. Department of Energy (DOE)–office of Basic Energy Sciences, Division of Chemical Sciences, Geosciences, and Biosciences under award DE-FG02-12ER16286. We used resources of the National Energy Research Scientific Computing Center (DOE contract DE-AC02-05CH11231) and the Terascale Infrastructure for Groundbreaking Research in Science and Engineering High-Performance Computer Center at Princeton University.

Supplementary Materials
www.sciencemag.org/cgi/content/full/341/6149/988/DC1
Materials and Methods
Supplementary Text
Figs. S1 to S11
Tables S1 and S2
References (*28*–*30*)
Movies S1 and S2

30 April 2013; accepted 2 August 2013
10.1126/science.1239879

Electron Acceleration in the Heart of the Van Allen Radiation Belts

G. D. Reeves,[1]* H. E. Spence,[2] M. G. Henderson,[1] S. K. Morley,[1] R. H. W. Friedel,[1] H. O. Funsten,[1] D. N. Baker,[3] S. G. Kanekal,[4] J. B. Blake,[5] J. F. Fennell,[5] S. G. Claudepierre,[5] R. M. Thorne,[6] D. L. Turner,[7] C. A. Kletzing,[8] W. S. Kurth,[8] B. A. Larsen,[1] J. T. Niehof[1]

The Van Allen radiation belts contain ultrarelativistic electrons trapped in Earth's magnetic field. Since their discovery in 1958, a fundamental unanswered question has been how electrons can be accelerated to such high energies. Two classes of processes have been proposed: transport and acceleration of electrons from a source population located outside the radiation belts (radial acceleration) or acceleration of lower-energy electrons to relativistic energies in situ in the heart of the radiation belts (local acceleration). We report measurements from NASA's Van Allen Radiation Belt Storm Probes that clearly distinguish between the two types of acceleration. The observed radial profiles of phase space density are characteristic of local acceleration in the heart of the radiation belts and are inconsistent with a predominantly radial acceleration process.

Radial diffusion of geomagnetically trapped electrons occurs continuously in Earth's time-varying magnetic field. Early theories of the formation of the Van Allen radiation belts focused on betatron and Fermi acceleration processes that act when electrons are transported from the outer magnetosphere where magnetic fields are weak (<100 nT) to the radiation belts, in the inner magnetosphere, where the magnetic fields are strong (*1*, *2*). The single-point measurements and low time resolution of early satellite observations suggested that radial diffusion could generally explain the equilibrium structure of the radiation belts and its evolution on the longer time scales (days to weeks) revealed in early satellite observations. In the 1990s, a growing network of satellites provided multipoint measurements with temporal and spatial resolutions, revealing complex structure and rapid dynamics that were difficult to explain with conventional theory.

In January 1997, a solar coronal mass ejection produced a strong geomagnetic storm and a dramatic intensification of radiation belt electron fluxes at energies up to several MeV (*3*, *4*). Comparison of the dynamics at geosynchronous orbit [~$6.6R_E$ (R_E is Earth's radius, 6372 km) or 42,000 km geocentric distance] and in the heart of the electron belt (~$4.2R_E$ or 27,000 km) showed that the intensification of relativistic electron fluxes occurred first in the heart of the belts and on extremely rapid time scales (~12 hours) and only later and more slowly at higher altitudes. In contrast with radial diffusion theory, these observations strongly suggested an energization process operating locally in the heart of the radiation belts (*3*). A leading candidate for that process was proposed to be acceleration by resonant interactions between radiation belt electrons and naturally occurring electromagnetic very low frequency (VLF) (≳ 1 kHz, i.e., radio) waves (*5*–*10*). However, around the same time other observations (*11*) showed a strong correlation between radiation belt electron enhancements and the power in global ultralow frequency (ULF) waves, which are enhanced during geomagnetic storms. Subsequent studies suggested that rapid enhancements of the radiation belts could be explained by acceleration from rapid, time-varying radial diffusion driven by the strong ULF field fluctuations (*12*–*17*).

Measurements of electron flux (electrons cm^{-2} s^{-1} sr^{-1} MeV^{-1}) cannot distinguish between local acceleration and acceleration by radial transport because both can produce radial peaks in electron flux. However, phase space density, which is the

[1]Space Science and Applications Group, Los Alamos National Laboratory, Los Alamos, NM 87545, USA. [2]Each Institute for the Study of Earth Oceans and Space, University of New Hampshire, Durham, NH 03824, USA. [3]Laboratory for Atmospheric and Space Research, University of Colorado, Boulder, CO 80309, USA. [4]NASA Goddard Space Flight Center, Greenbelt, MD 20771, USA. [5]The Aerospace Corporation, El Segundo, CA 90245, USA. [6]Department of Atmospheric and Ocean Sciences, University of California, Los Angeles, CA 90095, USA. [7]Department of Earth and Space Sciences, University of California, Los Angeles, CA 90095, USA. [8]Department of Physics, University of Iowa, Iowa City, IA 52242, USA.

*Corresponding author. E-mail: reeves@lanl.gov

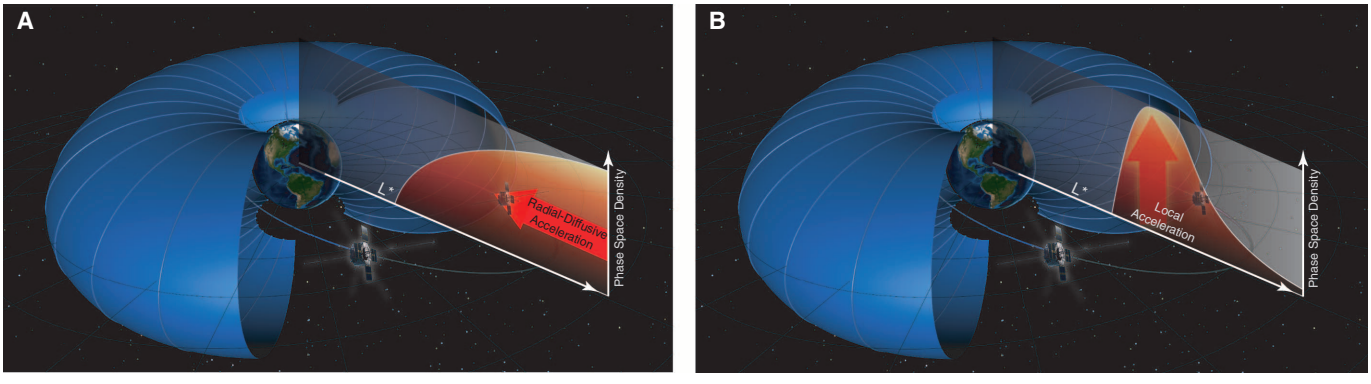

Fig. 1. The geometry of the radiation belts and RBSP orbits shown to scale. The positions of the RBSP satellites at 07:57 UT on 9 October are indicated. Also shown, in a cut-away view, is a single drift shell for electrons with 15° equatorial pitch angles starting at the position of RBSP-A at a radial distance $L^* \approx 4.2$. Representative magnetic field lines are plotted in light blue between the northern and southern magnetic mirror points. The radial profiles of phase space density expected from radial-diffusive acceleration (**A**) and local wave-particle acceleration (**B**) are indicted schematically.

ERRATUM

In the Report "Reaction of O_2 with Subsurface Oxygen Vacancies on TiO_2 Anatase (101)," new results indicate that the species referred as $(O_2^-)_{ads}$ is an adsorbed water molecule, and the species named $(O_2^{2-})_{ads}$ is a terminal OH group. Revisited identification of the species is described in Setvín *et al.*, *Phys. Chem. Chem. Phys.* **16**, 21524 (2014). The field-induced oxygen vacancy migration remains valid as described in the Report; the process is discussed in detail in Setvín *et al.*, *Phys. Rev. B* **91**, 195403 (2015). All theoretical results, notably the pathway in Figure 1, remain valid as well.

Science

Reaction of O_2 with Subsurface Oxygen Vacancies on TiO_2 Anatase (101)

Martin Setvín, Ulrich Aschauer, Philipp Scheiber, Ye-Fei Li, Weiyi Hou, Michael Schmid, Annabella Selloni and Ulrike Diebold

Science **341** (6149), 988-991.
DOI: 10.1126/science.1239879

Oxide Chemistry Below the Surface

Although metal oxides, such as titanium dioxide (TiO_2), are used for catalytic oxidation reactions and photocatalysis, the O_2 does not react directly with substrates. Vacancies in the surface region of the TiO_2 rutile phase can transfer a negative charge to adsorbed O_2 to create more reactive species. By contrast, in anatase—the phase associated with nanoscale TiO_2 particles—subsurface vacancies form. **Setvin *et al.*** (p. 988) used a scanning tunneling microscopy tip to pull these vacancies to the surface in a niobiumdoped anatase crystal and followed the transformation of adsorbed O_2^- into a peroxo species and a bridging O_2 dimer.